
LDPKiT: Recovering Utility in LDP Schemes by Training with Noise²

Kexin Li^{1†} Yang Xi¹ Aastha Mehta² David Lie¹
¹University of Toronto ²The University of British Columbia

Abstract

The adoption of large cloud-based models for inference has been hampered by concerns about the privacy leakage of end-user data. One method to mitigate this leakage is to add local differentially private noise to queries before sending them to the cloud, but this degrades utility as a side effect. Our key insight is that knowledge available in the noisy labels returned from performing inference on noisy inputs can be aggregated and used to recover the correct labels. We implement this insight in LDPKiT, which stands for *Local Differentially-Private and Utility-Preserving Inference via Knowledge Transfer*. LDPKiT uses the noisy labels returned from querying a set of *noised* inputs to train a local model (*noise*²), which is then used to perform inference on the original set of inputs. Our experiments on CIFAR-10, Fashion-MNIST, SVHN, and CARER NLP datasets demonstrate that LDPKiT can improve utility without compromising privacy. For instance, on CIFAR-10, compared to a standard ϵ -LDP scheme with $\epsilon = 15$, which provides a weak privacy guarantee, LDPKiT can achieve nearly the same accuracy (within 1% drop) with $\epsilon = 7$, offering an enhanced privacy guarantee. Moreover, the benefits of using LDPKiT increase at higher, more privacy-protective noise levels. For Fashion-MNIST and CARER, LDPKiT’s accuracy on the sensitive dataset with $\epsilon = 7$ not only exceeds the average accuracy of the standard ϵ -LDP scheme with $\epsilon = 7$ by roughly 20% and 9% but also outperforms the standard ϵ -LDP scheme with $\epsilon = 15$, a scenario with less noise and minimal privacy protection. We also perform *Zest* distance measurements to demonstrate that the type of distillation performed by LDPKiT is different from a model extraction attack.

1 Introduction

Cloud providers, such as Google, Amazon, and Microsoft, offer MLaaS (Machine Learning as a Service) [46], which enables the use of large, feature-rich ML models in several privacy-sensitive applications, such as personalized medicine and medical imaging [13], mobile healthcare apps, and surveillance [56]. At the same time, privacy concerns surrounding the MLaaS platforms arise during the widespread adoption and use of MLaaS. While users have privacy concerns regarding both training and inference stages of MLaaS platforms [17, 16, 3, 55], in this work, we focus on privacy concerns with regard to the inference services.

A malicious MLaaS provider can monitor or inspect a user’s queries during inference and use the information for purposes the user did not consent to. In 2016, for instance, Yahoo secretly complied with the US government’s digital communication surveillance and used its custom spam and child pornography detection system to monitor users’ emails [51, 7, 25]. More recently, the Amazon Ring Doorbell was found to have disclosed users’ video and audio footage to the police without authorization [36]. Ever since large language models have gained popularity, many organizations

[†]Corresponding author

have banned their members from using them due to the fear of data leakage [45, 14]. Even with a trusted provider, a compromised platform could enable an adversary to infer users’ queries via side-channels [66].

To tackle these privacy concerns, previous work has proposed applying homomorphic encryption schemes [8, 24] or hardware-enforced trusted execution environment [58] to protect inputs during inference. However, both schemes are primarily designed to protect against a malicious platform and implicitly trust the ML model provider—a malicious model can still leak arbitrary information about its inputs and would require some form of auditing. In addition, hardware-based schemes are prone to side-channel attacks [32, 61, 52], while homomorphic schemes can impose large overheads. An alternative to these schemes, which does not trust the entire model or platform and imposes virtually no performance overhead, is local differential privacy (LDP), which adds random LDP-provable noise to each of the user’s queries before transmitting them to the cloud for inference [29]. However, this “standard” application of LDP noise to the ML model’s inputs results in noise in the model outputs, leading to loss of utility.

We propose LDPKiT, which stands for *Local Differentially-Private and Utility-Preserving Inference via Knowledge Transfer*, a privacy-protective framework that recovers utility by training a local model. In standard applications of LDP, each query is independent, and information from the model’s prediction on one query does not help improve its predictions for others. Rather than being content with the loss of utility of each query individually, LDPKiT records both the (noised) query inputs and the (noisy and erroneous) labels returned from the cloud model (*i.e.*, *noise*²) to form a private training set, which is used to train a local model. As a result, LDPKiT’s training of a local model enables it to leverage collective knowledge from a batch of queries to improve the overall utility. However, if the local model is trained on too few points, its accuracy may not be sufficient to exceed that of using the labels directly from the standard usage of LDP. Thus, there exists a lower bound on the number of queries the user is willing to make for LDPKiT to be practical. Finally, one might wonder whether, as the number of points used to train the local model increases, it will ever become competitive with the cloud model—in other words, is this a type of model extraction attack? To study this, we also compare the local model with the cloud model and measure their model distances using the *Zest* framework [22].

Our analysis is guided by the following research questions:

RQ1. Does LDPKiT recover utility impacted by LDP noise?

RQ2. How does the number of queries impact LDPKiT?

RQ3. How does LDPKiT differ from an adversarial model extraction attack?

Contributions. To the best of our knowledge, we are the first to incorporate knowledge transfer techniques for privacy protection. With the (noisy) knowledge gained from the cloud model on privacy-preserving (noised) queries, LDPKiT can achieve high inference accuracy and mitigate privacy risks for sensitive queries. We evaluate LDPKiT on two modalities—image and text—with multiple models and datasets. We compare the privacy and inference accuracy tradeoffs of the local model trained using LDPKiT with the standard privacy-preserving inference scheme.

2 Related work

Knowledge transfer techniques. Knowledge distillation is a knowledge transfer technique that distills a large teacher model into a smaller student model while preserving model performance [20, 15, 48, 65, 68, 60, 44]. The conventional use case is model compression, enabling the model deployment in a resource-restricted environment. Knowledge can be transferred in different forms, such as logits, model parameters, intermediate layers’ activations or features, and their interrelationships [15]. Knowledge transfer also has adversarial applications. A model extraction attack is an adversarial example in which the attacker reproduces a model stealthily by stealing its parameters, decision boundaries, or functionalities. It demonstrates that an iterative query-based knowledge transfer process from a high-performance model can be performed via a prediction query interface [57, 69, 28]. Extraction can be successful with partial or zero knowledge of the victim model and training data [42, 69, 59, 41, 38]. Related defences [6, 2, 11, 31] and analyses [10, 5] are also in active research. Rather than model compression or extraction, we incorporate knowledge transfer for

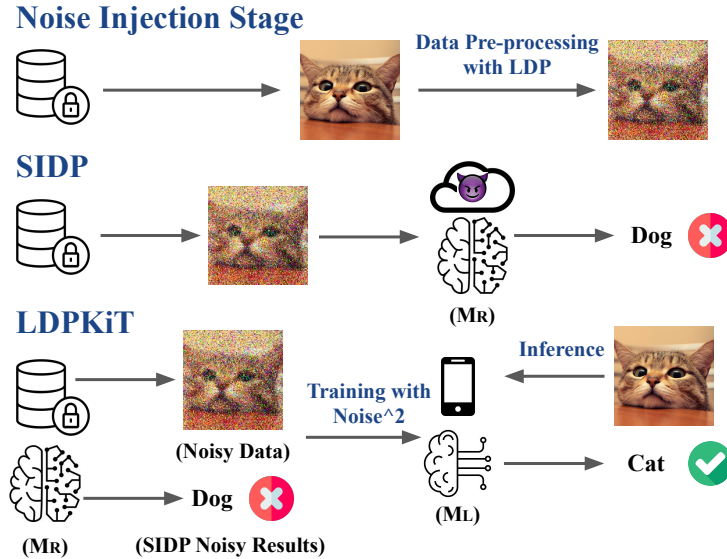


Figure 1: LDPKiT system overview.

privacy preservation in a non-adversarial manner to recover the utility loss brought by LDP. We quantitatively demonstrate that LDPKiT differs from the model extraction attack in Section 4.4.

Noise injection and differential privacy (DP). DP can be used either locally [12] or globally [43, 1, 72], and both methods provide provable privacy guarantees. Global differential privacy (GDP) shares original input data with a trusted data curator, which then applies noise to the aggregated data. In this case, the curator has access to the original sensitive data. To remove this point of trust, LDPKiT uses a local differential privacy (LDP) mechanism. In LDP, the data source (*i.e.*, the user) adds noise to each individual query before data transmission to the cloud, so she has full control over privacy protection. The side effect is that the noise is aggregated on the cloud, so LDP methods usually provide lower utility than GDP at the same level of privacy protection (*i.e.*, noise level). While we add noise to original inputs before offloading inference to the cloud, similar to [29], noise can also be injected into inference frameworks deployed on a split computation setting [33, 34, 40, 63], where the DNN is partitioned between the cloud and edge devices. These schemes involve a white-box model, so noise can be added to intermediate representations, which is different from our setting. A common challenge of DP schemes is to find a balance between utility and privacy.

Other privacy protection techniques. One class of privacy protection methods is data encryption with homomorphic algorithms, which suffers from high computational overheads [8, 24]. In contrast, LDPKiT is more efficient, as it does not require complicated computation to be performed for each query. Hardware-assisted inference in Trusted Execution Environments (TEEs) is another approach [58]. A TEE is a secure area within a processor that provides a safe environment for sensitive code execution, preventing unauthorized access. Slalom puts the computation in a TEE to address inference privacy on remote services [58]. However, Slalom does not protect against the risks of side-channel attacks. Since TEEs have access to the original data, privacy breaches can still happen if the attackers compromise the TEEs [61, 52, 30]. Side-channels are not a threat for LDPKiT since it does not transmit the original data, and any privacy leakage is bounded by the LDP noise.

3 Design

3.1 Threat model and preliminaries

Our goals are to protect sensitive user queries when using an ML cloud service and to recover some accuracy loss due to privacy-protective LDP noise added to the queries. We assume the cloud model provider is honest but curious. It honestly answers the user’s queries but may record both the queries

and their results to infer information about the user. We also restrict access to the cloud model by assuming that the cloud model returns hard labels only, which makes knowledge transfer more difficult [57, 21]. Throughout this paper, we use \mathcal{M}_R to denote the cloud-hosted model and \mathcal{M}_L to denote the local model hosted by the user. We use $\mathcal{D}_{\text{priv}}$ to denote the sensitive dataset for which the user wishes to query and attain labels from \mathcal{M}_R . Note that $\mathcal{D}_{\text{priv}}$ can be a predefined or dynamically generated set of points. We denote the number of queries (*i.e.*, size of $\mathcal{D}_{\text{priv}}$) as $|\mathcal{D}_{\text{priv}}|$. We use *SIDP* to denote the standard privacy-preserving inference scheme with LDP where noise is added to queries before sending them to \mathcal{M}_R , and \mathcal{M}_R returns noisy prediction results (with some errors) on the noisy queries.

Figure 1 presents an overview of LDPKiT, which has three stages: noise injection, remote inference (SIDP), and local training. Prior to querying \mathcal{M}_R for inference, LDPKiT adds ϵ -LDP [9] or ϵ -Utility-optimized Metric LDP (UMLDP) noise to the sensitive data points in $\mathcal{D}_{\text{priv}}$, depending on the modality. Once \mathcal{M}_R returns inference results, LDPKiT enters the local training stage. We elaborate on our design in the following subsections.

3.2 Noise injection

LDPKiT adds Laplacian noise to the sensitive queries in $\mathcal{D}_{\text{priv}}$ to obtain the ϵ -LDP guarantee [9] for image data and conducts text sanitization with ϵ -UMLDP privacy guarantee [67] for textual data, which are defined as follows.

Definition 3.1. ϵ -Local Differential Privacy (LDP). We define ϵ -LDP as follows [9]: A randomized algorithm \mathcal{A} satisfies ϵ -LDP if for all pairs of values and all sets \mathcal{S} of possible outputs, where $\mathcal{S} \subseteq \text{Range}(\mathcal{A})$,

$$\Pr[\mathcal{A}(v_1) \in \mathcal{S}] \leq e^\epsilon \Pr[\mathcal{A}(v_2) \in \mathcal{S}] \quad (1)$$

A lower ϵ value indicates a tighter bound of the equation and a stronger privacy guarantee.

Definition 3.2. Laplacian Mechanism. The Laplacian mechanism of LDP adds noise drawn from the Laplacian distribution, with the probability density function (PDF) defined as follows for a variable z and a scaling factor λ :

$$L(z, \lambda) = \frac{1}{2\lambda} \exp\left(-\frac{|z|}{\lambda}\right) \quad (2)$$

We prove that LDPKiT’s noise injection scheme satisfies the definition of ϵ -LDP with the Laplacian mechanism in Appendix A.

Laplacian noise is suitable for certain types of data, such as images. However, it would severely damage the semantic meaning of textual data because they are context-dependent and discrete. Hence, we use ϵ -UMLDP [67], an LDP notion tailored for NLP tasks with promising model accuracy (utility). ϵ -UMLDP [67] performs text sanitization on a vocabulary V by splitting V into sensitive (V_S) and insensitive (V_N) vocabularies based on the word rareness. The intuition is that insensitive words such as “a/an/the” are more frequently used in the English context. In contrast, sensitive words that contain private information such as birthdate, address, and password are used less frequently.

Definition 3.3. ϵ -UMLDP [67]. If the user has a sensitive word $x \in V_S$ and an insensitive word $y \in V_N$, The probability to replace x with y is as follows:

$$\Pr[M(x) = y] = C \cdot \frac{\exp(-\epsilon \cdot d(\phi(x), \phi(y)))}{\sum_{y' \in V_N} \exp(-\epsilon \cdot d(\phi(x), \phi(y')))} \quad (3)$$

where $d(\phi(x), \phi(y)) = 4 \left| \frac{1 - e^{\text{Cosine_Sim}(\phi(x), \phi(y)) - 1}}{e^{\text{Cosine_Sim}(\phi(x), \phi(y)) - 1} - 1} \right|$ and C is a constant normalization factor.

The complete proof of ϵ -UMLDP can be found in the original paper [67]. This normalized probability distribution provides ϵ -UMLDP privacy guarantee. It retains some semantic information for utility preservation by replacing the sensitive token x in V_S with the most semantically similar sanitized (insensitive) token y in V_N before sending it to an untrusted third party. We modify the original implementation of ϵ -UMLDP slightly to make the dataset-dependent ϵ values comparable to those used in the image analysis. The details and analyses of these changes are provided in Appendix B.

3.3 Privacy-preserving inference and local model training with noise²

When noise is added to a model input, it will translate into noise in the predicted label of the model output. One way to remove noise is through repeated queries, which is why most DP schemes define a “privacy budget” for repeated queries. Because the noise added by the LDP mechanism is independent of the underlying inputs, repeated queries to the cloud model with different random noise will progressively leak more information [23, 18]. Our intuition is that the repeated responses that the cloud model returns to the user should similarly leak more information about the “true label” that the cloud model would have predicted in the absence of LDP noise. We test this intuition by conducting a simple experiment on 100 random data samples in CIFAR-10 [27] with ResNet-152 (\mathcal{M}_R) and ResNet-18 (\mathcal{M}_L) [19]. We apply LDP noise on the 100 samples with ϵ set to 5 and repeatedly query each sample 5k times. Since \mathcal{M}_R returns different responses each time on the same samples with a different noise, these responses can “collaborate”, and the assembled knowledge can be transferred to \mathcal{M}_L throughout training. The experimental results show that \mathcal{M}_L gains enough knowledge about the original data samples to improve the prediction accuracy on them by 20%, from roughly 65% to 85%, which is close to \mathcal{M}_R ’s prediction accuracy on the un-noised $\mathcal{D}_{\text{priv}}$. It demonstrates that \mathcal{M}_L can learn to remove noise given noisy labels. However, repeatedly querying the same samples with noise will also leak private information about the samples to \mathcal{M}_R over time, which is undesirable. We, thus, investigate whether \mathcal{M}_L can learn about original samples when presented with noisy labels from querying *different* noisy samples. As a result, each element of $\mathcal{D}_{\text{priv}}$ is queried only once, with a single application of noise, thus preserving LDP privacy guarantees.

To realize our idea, LDPKiT first sends these privacy-preserved queries to \mathcal{M}_R and stores \mathcal{M}_R ’s predictions for further training on \mathcal{M}_L . LDPKiT trains \mathcal{M}_L with noised data from a sensitive dataset, $\mathcal{D}_{\text{priv}}$, and \mathcal{M}_R ’s noisy predictions on those noisy data (hence noise²). We then use \mathcal{M}_L to infer the correct labels on the original (noise-free) samples in $\mathcal{D}_{\text{priv}}$. LDPKiT can also be applied to an online learning setting where the user can iterate the entire process and periodically train \mathcal{M}_L using \mathcal{M}_R ’s predictions on new inference queries. Advanced ML training techniques such as active learning [54] and core-set strategies [53] can be used for query selection if $\mathcal{D}_{\text{priv}}$ is large.

4 Evaluation

In this section, we answer our three research questions (RQ1-3) in Section 1 with empirical analysis.

4.1 Experimental setup

We evaluate LDPKiT on two modalities: image and text. The ML models we use in image classification benchmarks are ResNet-152 (\mathcal{M}_R) [19], ResNet-18 (\mathcal{M}_L) [19] and MobileNetV2 (\mathcal{M}_L) [49]. We evaluate LDPKiT on three diverse datasets, namely CIFAR-10 [27], Fashion-MNIST [64], and SVHN [35]. For the NLP benchmark, we use a customized transformer-based model [62], where \mathcal{M}_R has two encoder blocks and \mathcal{M}_L has one, denoted as *Transformer_EN2* and *Transformer_EN1* (See Appendix C for specific architecture). We run the experiments on CARER’s emotion dataset [50].

As discussed in our setting, we have a sensitive dataset ($\mathcal{D}_{\text{priv}}$) of size $|\mathcal{D}_{\text{priv}}|$, and two parties are involved: \mathcal{M}_R deployed on a remote cloud and \mathcal{M}_L deployed on the user’s trusted local device. \mathcal{M}_L is a model randomly initialized with random weights. We assume that \mathcal{M}_R only returns the hard labels. The user’s goal is to obtain accurate predictions on the sensitive data points in $\mathcal{D}_{\text{priv}}$ from the cloud-hosted \mathcal{M}_R while minimizing privacy leakage.

We construct different \mathcal{M}_R for different tasks and datasets. For image modality, we train ResNet-152 on 35k, 35k, and 48,257 data points for CIFAR-10, Fashion-MNIST, and SVHN, respectively. For text modality, we train *Transformer_EN2* on 210k data points for CARER. Then, we create $\mathcal{D}_{\text{priv}}$ and a validation dataset, denoted as \mathcal{D}_{val} , using the left-out portion of the datasets that are unseen by \mathcal{M}_R . \mathcal{D}_{val} is isolated from the training process and evaluates \mathcal{M}_L ’s generalizability on unseen data. For CIFAR-10, $\mathcal{D}_{\text{priv}}$ has 15k data points, and the \mathcal{D}_{val} has 10k data points. For Fashion-MNIST and SVHN, $|\mathcal{D}_{\text{priv}}|$ is 25k for both datasets, and the sizes of \mathcal{D}_{val} are 10k and 26,032, respectively. Since CARER has over 410k data points, about $5\times$ larger than image benchmarks, $\mathcal{D}_{\text{priv}}$, in this case, is larger, containing 70k data samples, and the \mathcal{D}_{val} has 10k samples. As a reference, when no privacy protection exists and thus no noise is added, \mathcal{M}_R ’s accuracies on $\mathcal{D}_{\text{priv}}$ of CIFAR-10, Fashion-MNIST, SVHN, and CARER are 87.85%, 93.49%, 95.20%, and 91.00%. The accuracies on

\mathcal{D}_{val} are 87.10%, 93.22%, 96.30%, and 90.00%, respectively. For all the experiments, we gradually expand $\mathcal{D}_{\text{priv}}$ and train \mathcal{M}_L on noisy data and labels iteratively to study the effect of $|\mathcal{D}_{\text{priv}}|$. In each iteration, LDPKiT randomly selects a small batch of samples from $\mathcal{D}_{\text{priv}}$ (1.5k for CIFAR-10, 2.5k for Fashion-MNIST and SVHN, and 7k for CARER NLP benchmark), adds LDP noise, and then sends them to \mathcal{M}_R to attain noisy labels. The ϵ values we present in our evaluation are 15, 10, 7, 5, and 3 across all the benchmarks, which are generally accepted by the industry standard [4, 39]. We collect and report \mathcal{M}_L 's accuracies on the original samples in $\mathcal{D}_{\text{priv}}$ and \mathcal{D}_{val} , where \mathcal{M}_L is trained on noisy data from $\mathcal{D}_{\text{priv}}$ with different noise levels (noise^2).

We run our experiments on two machines. One has two GPUs with models NVIDIA GeForce RTX 3090 and 4090 with 24GB of dedicated memory and an Intel 12th Gen i7-12700 CPU with 12 cores and 64GB of RAM. The other has two NVIDIA GeForce RTX 4090 GPUs and an AMD Ryzen Threadripper PRO 5955WX CPU with 16 cores and 64GB of RAM. The underlying OS are 64-bit Ubuntu 22.04.3 LTS and Ubuntu 24.04 LTS, respectively. We use Python 3.9.7 and PyTorch v2.1.2 with CUDA 12.1. All experiments are repeated over three random seeds to determine the statistical significance of our findings. We conduct the dependent two-sample t-test on our results and collect the p values. We find that most of the improvements are statistically significant (*i.e.*, $p < 0.05$) with few outliers. We mark the accuracies that have $p > 0.05$ with an asterisk (*) in Tables 2 and 3. We document the hyperparameters used and dataset preparation details in Appendix D.

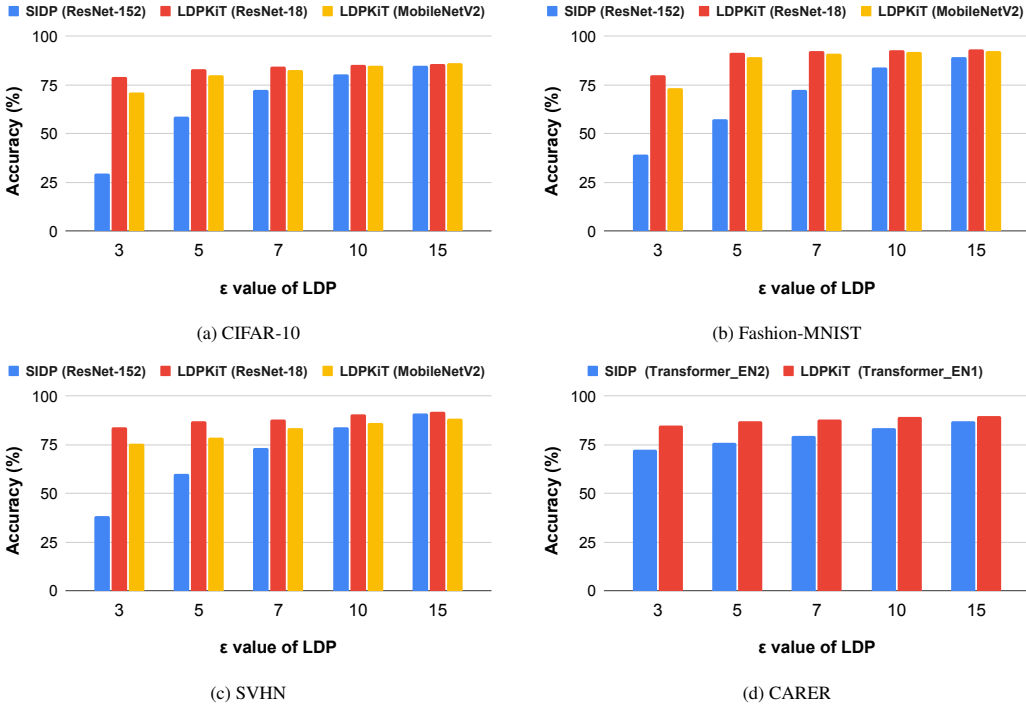
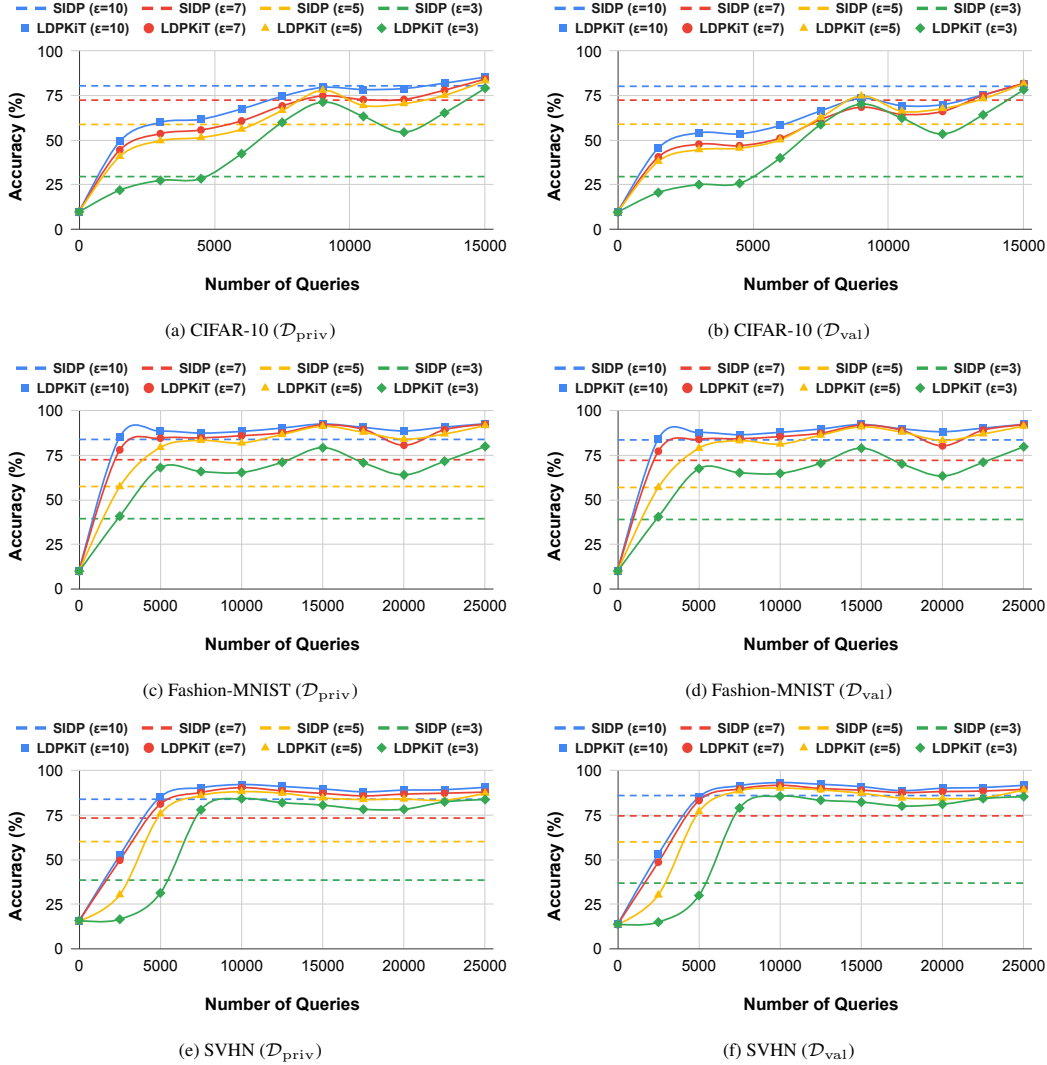


Figure 2: Comparison of accuracies on $\mathcal{D}_{\text{priv}}$ between SIDP and LDPKiT with different ϵ values.

4.2 RQ1: Utility recovery

We record the final accuracies on the entire $\mathcal{D}_{\text{priv}}$ at the last epoch of training (*i.e.*, 15k for CIFAR-10, 25k for Fashion-MNIST and SVHN, and 70k for CARER) and show the difference of final accuracies on $\mathcal{D}_{\text{priv}}$ between SIDP and LDPKiT in Figure 2. Our results show that LDPKiT can almost always achieve higher inference accuracy than SIDP, except in a few cases when the least noise is added (*i.e.*, $\epsilon = 15$). However, there is barely privacy protection in the case of $\epsilon = 15$ (See Appendix E for samples with different noise levels). As more LDP noise is added to $\mathcal{D}_{\text{priv}}$ to preserve privacy, the gap in utility that LDPKiT provides over SIDP also increases. Therefore, LDPKiT offers greater benefits in regimes with stronger privacy protection and correspondingly more noise.

In contrast, when privacy protection is weak, and the ϵ value is high (e.g., $\epsilon = 15$), LDPKiT’s improvement becomes trivial. We tabulate the numerical accuracies on $\mathcal{D}_{\text{priv}}$ obtained in our experiments in Table 2 in the appendix. Our experiments show that LDPKiT provides better privacy with essentially no loss of accuracy compared to SIDP. For instance, on CIFAR-10 with ResNet-18, SIDP provides an average accuracy of 84.78% at $\epsilon = 15$, while LDPKiT is able to provide a roughly equivalent accuracy of 83.27% for a much stronger level of privacy at $\epsilon = 5$. In contrast, at the same level of privacy of $\epsilon = 5$, SIDP only achieves an average accuracy of 58.76% by comparison. Similarly, for CARER, SIDP provides an accuracy of 87.12% at $\epsilon = 15$, while LDPKiT achieves an accuracy of 84.75% at $\epsilon = 3$. This trend is also present in Fashion-MNIST and SVHN. The experimental results demonstrate that LDPKiT can recover a majority of the utility loss due to the addition of LDP noise.



SIDP lines in the plots give the average accuracy across all queries at a given ϵ .

Figure 3: ResNet-18’s accuracies on $\mathcal{D}_{\text{priv}}$ and \mathcal{D}_{val} of CIFAR-10, Fashion-MNIST and SVHN.

4.3 RQ2: Influence of $|\mathcal{D}_{\text{priv}}|$ on LDPKiT

Figure 3 and Appendix F.1 illustrate the accuracy of \mathcal{M}_L on $\mathcal{D}_{\text{priv}}$ and \mathcal{D}_{val} as a function of $|\mathcal{D}_{\text{priv}}|$ at various values of ϵ , along with the average accuracy of SIDP on $\mathcal{D}_{\text{priv}}$ at the same values of ϵ (as dotted lines). We observe that accuracies on $\mathcal{D}_{\text{priv}}$ and \mathcal{D}_{val} both exhibit similar and increasing accuracies as $|\mathcal{D}_{\text{priv}}|$ increases. Moreover, we observe that for each noise level, there exists a lower

bound of $|\mathcal{D}_{\text{priv}}|$, *i.e.*, a *cross-over* point, where the increasing LDPKiT accuracy (solid lines) exceeds the average SIDP accuracy (dotted lines). When $|\mathcal{D}_{\text{priv}}|$ is too small, it is not sufficient to train a \mathcal{M}_L that can outperform SIDP. Hence, $|\mathcal{D}_{\text{priv}}|$ needs to be larger than this cross-over point for LDPKiT to be beneficial. We notice that the $|\mathcal{D}_{\text{priv}}|$ where the cross-over point occurs is dataset-dependent. For CIFAR-10 and CARER, the cross-over points are lower when more noise is added. In other words, fewer queries are needed for LDPKiT to outperform SIDP in a more privacy-protective setting. As shown in the subplot (a) of Figure 3, the cross-over point for ResNet-18 on CIFAR-10 ($\mathcal{D}_{\text{priv}}$) is around 5k queries when $\epsilon = 3$. The cross-over point increases to 8k when $\epsilon = 5$ and to more than 12k when $\epsilon = 10$. In contrast, we observe a different trend for Fashion-MNIST and SVHN. In these cases, the cross-over points are similar across all ϵ values. For instance, the cross-over points for Fashion-MNIST are around 2.5k for all ϵ , and for SVHN, the cross-over points are around 5k for ResNet-18 and 2.5k for MobileNetV2. We even notice a few instances where a cross-over point occurs at a smaller $|\mathcal{D}_{\text{priv}}|$ when less noise is added. For example, the cross-over point for SVHN occurs around 4k for $\epsilon = 5$ and over 5k for $\epsilon = 3$. Overall, fewer queries are generally needed for LDPKiT accuracy to exceed the average SIDP accuracy compared to CIFAR-10 and CARER. We suspect these differences can be attributed to Fashion-MNIST and SVHN being easier to train ML models on and, thus, having accuracies on these datasets that increase faster relative to the size of $\mathcal{D}_{\text{priv}}$. However, further investigation is needed to fully explain this dataset-dependent difference.

One may argue that LDPKiT’s effectiveness is highly dependent on $|\mathcal{D}_{\text{priv}}|$ and $|\mathcal{D}_{\text{priv}}|$ should be as high as possible to make LDPKiT become beneficial. This is not true because LDP only bounds privacy leakage—it does not make it non-existent—so every additional query the user makes still leaks some amount of information. On the other hand, the gains in \mathcal{M}_L accuracy see diminishing returns at large $|\mathcal{D}_{\text{priv}}|$. Therefore, the user may wish to set an upper bound of $|\mathcal{D}_{\text{priv}}|$, *i.e.*, a *stopping* point, based on their desire for privacy and the decreasing benefits of querying \mathcal{M}_R for LDPKiT. We observe that more queries are required for cases with higher and more privacy-protective noise levels to reach this upper bound across all the benchmarks. Training on Fashion-MNIST and SVHN reaches such an upper bound at a relatively earlier stage compared to other datasets, *i.e.*, the accuracy remains high (saturates) after about 5k queries are made, except for the case $\epsilon = 3$ in SVHN. Again, we believe that it is because they are relatively easier datasets to train models for compared to CIFAR-10. One way for the user to determine the stopping point to prevent further privacy leakage is to monitor the accuracy on a small labeled \mathcal{D}_{val} . For instance, when \mathcal{M}_L has a decent accuracy on \mathcal{D}_{val} and increasing $|\mathcal{D}_{\text{priv}}|$ brings minimal accuracy improvement on \mathcal{D}_{val} , the user can stop querying \mathcal{M}_R and rely on \mathcal{M}_L for predictions so long as future samples fall in the same distribution as $\mathcal{D}_{\text{priv}}$.

We tabulate the detailed accuracies on $\mathcal{D}_{\text{priv}}$ and \mathcal{D}_{val} in Appendices F.2 and F.3. The experimental results show that LDPKiT has greater benefits when more LDP noise is added (*i.e.*, stronger privacy protection). As Figures 3, 10 and 11 show, \mathcal{M}_L ’s accuracies on $\mathcal{D}_{\text{priv}}$ and \mathcal{D}_{val} illustrate similar trends. Hence, when $|\mathcal{D}_{\text{priv}}|$ is large enough, LDPKiT generates a trustworthy local model that can accurately predict unseen sensitive data points. The user can utilize the accuracy on a \mathcal{D}_{val} as a reference to determine the stopping point of querying \mathcal{M}_R to prevent further privacy leakage.

Table 1: Normalized Zest distance results with *Cosine* distance metric on \mathcal{M}_R and \mathcal{M}_L .

Dataset	\mathcal{M}_R	\mathcal{M}_L	LDP ($\epsilon=15$)	LDP ($\epsilon=10$)	LDP ($\epsilon=7$)	LDP ($\epsilon=5$)	LDP ($\epsilon=3$)
CIFAR-10	ResNet-152	ResNet-18	2.1063 (± 0.40)	1.7191 (± 0.01)	1.7566 (± 0.07)	1.7609 (± 0.15)	1.9074 (± 0.13)
		MobileNetV2	1.4735 (± 0.05)	1.5903 (± 0.02)	1.7406 (± 0.01)	1.8716 (± 0.08)	2.1970 (± 0.08)
Fashion-MNIST	ResNet-152	ResNet-18	1.1740 (± 0.08)	1.6653 (± 0.24)	1.9437 (± 0.19)	1.8752 (± 0.12)	2.5559 (± 0.14)
		MobileNetV2	1.0567 (± 0.07)	1.3772 (± 0.17)	1.9533 (± 0.12)	2.3278 (± 0.06)	2.7042 (± 0.10)
SVHN	ResNet-152	ResNet-18	1.2497 (± 0.13)	1.2374 (± 0.04)	1.2303 (± 0.07)	1.3165 (± 0.02)	1.4662 (± 0.07)
		MobileNetV2	1.2760 (± 0.03)	1.2664 (± 0.06)	1.3534 (± 0.13)	1.3507 (± 0.06)	1.4850 (± 0.01)

The values recorded in parentheses are the standard deviations of the accuracies.

4.4 RQ3: Difference from model extraction

Although our method requires knowledge transfer from a remote model to a local model, it is different from the adversarial model extraction attack [42, 69, 59, 41, 38]. LDPKiT has orthogonal goals. The motivations for model stealing are often cost-driven, and model stealers aim to replicate the victim model’s high performance with minimal queries, ensuring the theft requires less effort. In contrast,

our ultimate goal is to protect the privacy of inference data. The reason the user stops querying \mathcal{M}_R is not necessarily due to monetary concerns but to prevent further privacy leakage.

We answer RQ3 quantitatively using *Zest* distances [22] as our evaluation metrics, which are the distances between two models computed based on LIME’s model-agnostic explanations [47]. We use *Zest* because of its architecture independence, the model’s black-box access requirement, and its perfect accuracy in model extraction detection with *Cosine* distance metric. *Zest* supports l_1, l_2, l_∞ norm and *Cosine* distances. The authors of *Zest* claim that it is capable of detecting model extraction attacks with 100% accuracy when using *Cosine* distance [22], which is the metric we present in Table 1. The specific procedure of model extraction attack detection is presented in Appendix G.

We present the normalized *Zest* distances, \overline{D}_z , with the *Cosine* distance metric in Table 1. We present the results of the rest of the distance metrics supported by *Zest* in Appendix H. According to the paper [22], *Zest* also has text modality support. However, that part of the code is not released to the public, so we can only report the results on image modality in our paper. As explained in Appendix G, an adversarial model extraction attack occurs when $\overline{D}_z < 1$. Table 1 shows that LDPKiT does not contribute to model theft at any noise level since all $\overline{D}_z > 1$, and the distance increases as the noise level increases (*i.e.*, better privacy protection but farther from model extraction), which are the regimes that we expect LDPKiT to be used in.

From these results, we surmise that LDPKiT has several key differences from model stealing/extraction. First, one of the goals of a model extraction attack is to generate a model with similar performance as the victim model [57]. At fairly privacy-protective noise levels, such as $\epsilon = 7$ and $\epsilon = 5$, Resnet-18 trained on CIFAR-10 only achieves roughly 79% and 75% accuracy, respectively, while \mathcal{M}_R has an accuracy of 87%—a significant gap in performance. Notably, since \mathcal{M}_L is not competitive with \mathcal{M}_R , LDPKiT does not violate the terms of use for major commercial models [37]. Moreover, in LDPKiT, the user will stop training once accuracy gains diminish to protect privacy, so they are unlikely to achieve much higher accuracy. Second, model extraction attacks seek to maximize the accuracy of the extracted model with as few queries as possible. Efficient model extraction requires samples that are in the distribution of \mathcal{M}_R ’s training set [59]. Since LDPKiT queries inputs with noise added, they are not likely to be in the distribution \mathcal{M}_R is trained on and, thus, are not a query-efficient method for knowledge transfer. Finally, as demonstrated by our experiments with *Zest*, the extracted model does not behave very similarly to \mathcal{M}_R , and its main benefit is in recovering utility for $\mathcal{D}_{\text{priv}}$.

5 Discussion and limitations

In LDPKiT, instead of training \mathcal{M}_L with original samples, we train it on noised samples, as described in Section 3.3. Intuitively, the additive noise will likely change some of the features in the original samples, so the noised samples will more strongly correspond to the noised labels predicted by \mathcal{M}_R for knowledge transfer. We compare local training with noisy or original data samples and observe that training \mathcal{M}_L with noisy samples yields greater recovery of accuracy, especially when there is more noise. We present the results in Appendix I. Furthermore, since \mathcal{M}_L is trained on noisy data, LDPKiT is inherently immune to membership inference attacks if \mathcal{M}_L is ever leaked.

As for the limitations, due to time constraints, we only tested on supervised learning, specifically classification tasks. We may extend the evaluation to regression tasks or unsupervised clustering tasks in the future. Also, our privacy-preserving queries in this paper refer to queries with LDP noise applied. As a future direction, we can also compose our privacy-preserving $\mathcal{D}_{\text{priv}}$ by generating synthetic queries or selecting similar queries from public datasets based on similarity metrics. Moreover, LDPKiT is compatible with advanced training strategies, such as active learning, that expedite model training. We plan to study the effect of such strategies on LDPKiT in the future.

6 Conclusion

LDPKiT is an inference framework that preserves the privacy of data in a sensitive dataset when using malicious cloud services by injecting LDP noise. Since all the privacy protection measures are applied before transmitting to the remote server, the protection still exists even if the cloud service is deployed on a compromised platform or the cloud model is leaked. The key insight is that partial knowledge about the real data, though noisy, still exists in the noisy labels returned from the cloud

model. LDPKiT put this insight into use by aggregating the partial knowledge from noisy queries and then training a local model with the knowledge. The experimental results demonstrate that LDPKiT can recover the prediction accuracy on private data throughout training while preserving privacy. LDPKiT has greater benefits when the noise level increases, which are the more privacy-protective regimes we expect LDPKiT to be used in. We also quantitatively demonstrate that the level of knowledge transfer in LDPKiT does not construct an adversarial model extraction attack.

References

- [1] ABADI, M., CHU, A., GOODFELLOW, I., MCMAHAN, H. B., MIRONOV, I., TALWAR, K., AND ZHANG, L. Deep Learning with Differential Privacy. In *Proceedings of the 2016 ACM SIGSAC Conference on Computer and Communications Security* (oct 2016), ACM.
- [2] ADI, Y., BAUM, C., CISSE, M., PINKAS, B., AND KESHET, J. Turning Your Weakness Into a Strength: Watermarking Deep Neural Networks by Backdooring, 2018.
- [3] AL-RUBAIE, M., AND CHANG, J. M. Privacy-preserving machine learning: Threats and solutions. *IEEE Security & Privacy* 17, 2 (2019), 49–58.
- [4] APPLE. Differential Privacy. https://www.apple.com/privacy/docs/Differential_Privacy_Overview.pdf.
- [5] CHANDRASEKARAN, V., CHAUDHURI, K., GIACOMELLI, I., JHA, S., AND YAN, S. Exploring Connections between Active Learning and Model Extraction. In *Proceedings of the 29th USENIX Conference on Security Symposium (USA, 2020)*, SEC’20, USENIX Association.
- [6] CHEN, H., ROUHANI, B. D., FU, C., ZHAO, J., AND KOUSHANFAR, F. DeepMarks: A Secure Fingerprinting Framework for Digital Rights Management of Deep Learning Models. In *Proceedings of the 2019 on International Conference on Multimedia Retrieval (New York, NY, USA, 2019)*, ICMR ’19, Association for Computing Machinery, p. 105–113.
- [7] DAVE, P., AND BENNET, B. Yahoo helped the U.S. Government spy on emails, report says, Oct 2016.
- [8] DOWLIN, N., GILAD-BACHRACH, R., LAINE, K., LAUTER, K., NAEHRIG, M., AND WERNING, J. CryptoNets: Applying Neural Networks to Encrypted Data with High Throughput and Accuracy. Tech. Rep. MSR-TR-2016-3, February 2016.
- [9] DWORK, C., MCSHERRY, F., NISSIM, K., AND SMITH, A. Calibrating noise to sensitivity in private data analysis. In *Theory of Cryptography: Third Theory of Cryptography Conference, TCC 2006, New York, NY, USA, March 4-7, 2006. Proceedings 3* (2006), Springer, pp. 265–284.
- [10] DZIEDZIC, A., DHAWAN, N., KALEEM, M. A., GUAN, J., AND PAPERNOT, N. On the Difficulty of Defending Self-Supervised Learning against Model Extraction, 2022.
- [11] DZIEDZIC, A., KALEEM, M. A., LU, Y. S., AND PAPERNOT, N. Increasing the Cost of Model Extraction with Calibrated Proof of Work, 2022.
- [12] ERLINGSSON, U., PIHUR, V., AND KOROLOVA, A. RAPPOR: Randomized Aggregatable Privacy-Preserving Ordinal Response. In *Proceedings of the 2014 ACM SIGSAC Conference on Computer and Communications Security (New York, NY, USA, 2014)*, CCS ’14, Association for Computing Machinery, p. 1054–1067.
- [13] ESTEVA, A., ROBICQUET, A., RAMSUNDAR, B., KULESHOV, V., DEPRISTO, M., CHOU, K., CUI, C., CORRADO, G., THRUN, S., AND DEAN, J. A guide to deep learning in healthcare. *Nature medicine* 25, 1 (2019), 24–29.
- [14] GORDON, N. Apple restricts employee chatgpt use as companies worry about data leaks, May 2023.
- [15] GOU, J., YU, B., MAYBANK, S. J., AND TAO, D. Knowledge Distillation: A Survey. *Int. J. Comput. Vision* 129, 6 (jun 2021), 1789–1819.
- [16] HAMZA, Y. A., AND OMAR, M. D. Cloud computing security: abuse and nefarious use of cloud computing. *Int. J. Comput. Eng. Res* 3, 6 (2013), 22–27.
- [17] HANNUN, A., GUO, C., AND VAN DER MAATEN, L. Measuring data leakage in machine-learning models with Fisher information. In *Uncertainty in Artificial Intelligence (2021)*, PMLR, pp. 760–770.
- [18] HASSAN, U., AND ANWAR, M. S. Reducing noise by repetition: introduction to signal averaging. *European Journal of Physics* 31, 3 (2010), 453.
- [19] HE, K., ZHANG, X., REN, S., AND SUN, J. Deep Residual Learning for Image Recognition, 2015.
- [20] HINTON, G., VINYALS, O., AND DEAN, J. Distilling the knowledge in a neural network. *arXiv preprint arXiv:1503.02531* (2015).

- [21] JAGIELSKI, M., CARLINI, N., BERTHELOT, D., KURAKIN, A., AND PAPERNOT, N. High Accuracy and High Fidelity Extraction of Neural Networks, 2020.
- [22] JIA, H., CHEN, H., GUAN, J., SHAMSABADI, A. S., AND PAPERNOT, N. A Zest of LIME: Towards Architecture-Independent Model Distances. In *International Conference on Learning Representations* (2021).
- [23] JIANG, W., MA, Z., LI, S., XIAO, H., AND YANG, J. Privacy budget management and noise reusing in multichain environment. *International Journal of Intelligent Systems* 37, 12 (2022), 10462–10475.
- [24] JUVEKAR, C., VAIKUNTANATHAN, V., AND CHANDRAKASAN, A. Gazelle: A Low Latency Framework for Secure Neural Network Inference, 2018.
- [25] KAYE, D. Reports that Yahoo aided us e-mail surveillance draw concern of UN Human Rights Expert | UN News, Oct 2016.
- [26] KIM, S., LE, D., ZHENG, W., SINGH, T., ARORA, A., ZHAI, X., FUEGEN, C., KALINLI, O., AND SELTZER, M. L. Evaluating User Perception of Speech Recognition System Quality with Semantic Distance Metric, 2022.
- [27] KRIZHEVSKY, A., HINTON, G., ET AL. Learning multiple layers of features from tiny images.
- [28] LEE, S., LEE, G., KIM, J. W., SHIN, J., AND LEE, M.-K. HETAL: Efficient privacy-preserving transfer learning with homomorphic encryption. In *Proceedings of the 40th International Conference on Machine Learning* (23–29 Jul 2023), A. Krause, E. Brunskill, K. Cho, B. Engelhardt, S. Sabato, and J. Scarlett, Eds., vol. 202 of *Proceedings of Machine Learning Research*, PMLR, pp. 19010–19035.
- [29] LEROUX, S., VERBELEN, T., SIMOENS, P., AND DHOEDT, B. Privacy Aware Offloading of Deep Neural Networks, 2018.
- [30] LIPP, M., SCHWARZ, M., GRUSS, D., PRESCHER, T., HAAS, W., HORN, J., MANGARD, S., KOCHER, P., GENKIN, D., YAROM, Y., ET AL. Meltdown: Reading kernel memory from user space. *Communications of the ACM* 63, 6 (2020), 46–56.
- [31] LIU, Y., LI, K., LIU, Z., WEN, B., XU, K., WANG, W., ZHAO, W., AND LI, Q. Provenance of Training without Training Data: Towards Privacy-Preserving DNN Model Ownership Verification. In *Proceedings of the ACM Web Conference 2023* (New York, NY, USA, 2023), WWW ’23, Association for Computing Machinery, p. 1980–1990.
- [32] LOU, X., ZHANG, T., JIANG, J., AND ZHANG, Y. A Survey of Microarchitectural Side-channel Vulnerabilities, Attacks and Defenses in Cryptography, 2021.
- [33] LYU, L., BEZDEK, J. C., JIN, J., AND YANG, Y. FORESEEN: Towards Differentially Private Deep Inference for Intelligent Internet of Things. *IEEE Journal on Selected Areas in Communications* 38, 10 (2020), 2418–2429.
- [34] MIRESHGHALLAH, F., TARAM, M., RAMRAKHYANI, P., JALALI, A., TULLSEN, D., AND ESMAEILZADEH, H. Shredder: Learning noise distributions to protect inference privacy. In *Proceedings of the Twenty-Fifth International Conference on Architectural Support for Programming Languages and Operating Systems* (2020), pp. 3–18.
- [35] NETZER, Y., WANG, T., COATES, A., BISSACCO, A., WU, B., AND NG, A. Y. Reading digits in natural images with unsupervised feature learning.
- [36] NG, A. Amazon gave ring videos to police without owners’ permission, Jul 2022.
- [37] OPENAI. Terms of use. <https://openai.com/policies/terms-of-use/>.
- [38] OREKONDY, T., SCHIELE, B., AND FRITZ, M. Knockoff Nets: Stealing Functionality of Black-Box Models, 2018.
- [39] ORR, A. Google’s differential privacy may be better than Apple’s, Sep 2017.
- [40] OSIA, S. A., SHAHIN SHAMSABADI, A., SAJADMANESH, S., TAHERI, A., KATEVAS, K., RABIEE, H. R., LANE, N. D., AND HADDADI, H. A Hybrid Deep Learning Architecture for Privacy-Preserving Mobile Analytics. *IEEE Internet of Things Journal* 7, 5 (2020), 4505–4518.
- [41] PAL, S., GUPTA, Y., SHUKLA, A., KANADE, A., SHEVADE, S. K., AND GANAPATHY, V. Activethief: Model extraction using active learning and unannotated public data. In *The Thirty-Fourth AAAI Conference on Artificial Intelligence, AAAI 2020, The Thirty-Second Innovative*

Applications of Artificial Intelligence Conference, IAAI 2020, The Tenth AAAI Symposium on Educational Advances in Artificial Intelligence, EAAI 2020, New York, NY, USA, February 7-12, 2020 (2020), AAAI Press, pp. 865–872.

- [42] PAPERNOT, N., MCDANIEL, P., GOODFELLOW, I., JHA, S., CELIK, Z. B., AND SWAMI, A. Practical Black-Box Attacks against Machine Learning. In *Proceedings of the 2017 ACM on Asia Conference on Computer and Communications Security* (New York, NY, USA, 2017), ASIA CCS '17, Association for Computing Machinery, p. 506–519.
- [43] PAPERNOT, N., SONG, S., MIRONOV, I., RAGHUNATHAN, A., TALWAR, K., AND ÚLFAR ERLINGSSON. Scalable Private Learning with PATE, 2018.
- [44] PARK, W., KIM, D., LU, Y., AND CHO, M. Relational Knowledge Distillation. In *Proceedings of the IEEE/CVF Conference on Computer Vision and Pattern Recognition (CVPR)* (June 2019).
- [45] RAY, S. Apple joins a growing list of companies cracking down on use of chatgpt by staffers—here’s why, Oct 2023.
- [46] RIBEIRO, M., GROLINGER, K., AND CAPRETZ, M. A. MLaaS: Machine Learning as a Service. In *2015 IEEE 14th International Conference on Machine Learning and Applications (ICMLA)* (2015), pp. 896–902.
- [47] RIBEIRO, M. T., SINGH, S., AND GUESTRIN, C. "Why should i trust you?" Explaining the predictions of any classifier. In *Proceedings of the 22nd ACM SIGKDD international conference on knowledge discovery and data mining* (2016), pp. 1135–1144.
- [48] ROMERO, A., BALLAS, N., KAHOU, S. E., CHASSANG, A., GATTA, C., AND BENGIO, Y. FitNets: Hints for Thin Deep Nets, 2015.
- [49] SANDLER, M., HOWARD, A., ZHU, M., ZHMOGINOV, A., AND CHEN, L.-C. MobileNetV2: Inverted Residuals and Linear Bottlenecks, 2019.
- [50] SARAVIA, E., LIU, H.-C. T., HUANG, Y.-H., WU, J., AND CHEN, Y.-S. CARER: Contextualized affect representations for emotion recognition. In *Proceedings of the 2018 Conference on Empirical Methods in Natural Language Processing* (Brussels, Belgium, Oct.-Nov. 2018), Association for Computational Linguistics, pp. 3687–3697.
- [51] SAVAGE, C., AND PERLROTH, N. Yahoo said to have aided U.S. email surveillance by adapting spam filter, Oct 2016.
- [52] SCHWARZ, M., LIPP, M., MOGHIMI, D., VAN BULCK, J., STECKLINA, J., PRESCHER, T., AND GRUSS, D. ZombieLoad: Cross-privilege-boundary data sampling. In *Proceedings of the 2019 ACM SIGSAC Conference on Computer and Communications Security* (2019), pp. 753–768.
- [53] SENER, O., AND SAVARESE, S. Active learning for convolutional neural networks: A core-set approach. *arXiv preprint arXiv:1708.00489* (2017).
- [54] SETTLES, B. Active learning literature survey.
- [55] SHOKRI, R., STRONATI, M., SONG, C., AND SHMATIKOV, V. Membership Inference Attacks Against Machine Learning Models. In *2017 IEEE symposium on security and privacy (SP)* (2017), IEEE, pp. 3–18.
- [56] SINGH, A., PATIL, D., AND OMKAR, S. Eye in the Sky: Real-Time Drone Surveillance System (DSS) for Violent Individuals Identification Using ScatterNet Hybrid Deep Learning Network. In *2018 IEEE/CVF Conference on Computer Vision and Pattern Recognition Workshops (CVPRW)* (2018), pp. 1710–17108.
- [57] TRAMÈR, F., ZHANG, F., JUELS, A., REITER, M. K., AND RISTENPART, T. Stealing Machine Learning Models via Prediction APIs. In *USENIX security symposium* (2016), vol. 16, pp. 601–618.
- [58] TRAMÈR, F., AND BONEH, D. Slalom: Fast, Verifiable and Private Execution of Neural Networks in Trusted Hardware, 2019.
- [59] TRUONG, J.-B., MAINI, P., WALLS, R. J., AND PAPERNOT, N. Data-free model extraction. In *Proceedings of the IEEE/CVF conference on computer vision and pattern recognition* (2021), pp. 4771–4780.
- [60] TUNG, F., AND MORI, G. Similarity-preserving knowledge distillation. In *Proceedings of the IEEE/CVF International Conference on Computer Vision* (2019), pp. 1365–1374.

- [61] VAN BULCK, J., MINKIN, M., WEISSE, O., GENKIN, D., KASIKCI, B., PIESSENS, F., SILBERSTEIN, M., WENISCH, T. F., YAROM, Y., AND STRACKX, R. Foreshadow: Extracting the keys to the Intel SGX kingdom with transient Out-of-Order execution. In *27th USENIX Security Symposium (USENIX Security 18)* (2018), pp. 991–1008.
- [62] VASWANI, A., SHAZEER, N., PARMAR, N., USZKOREIT, J., JONES, L., GOMEZ, A. N., KAISER, L., AND POLOSUKHIN, I. Attention Is All You Need, 2023.
- [63] WANG, J., ZHANG, J., BAO, W., ZHU, X., CAO, B., AND YU, P. S. Not Just Privacy: Improving Performance of Private Deep Learning in Mobile Cloud, 2018.
- [64] XIAO, H., RASUL, K., AND VOLLGRAF, R. Fashion-mnist: a novel image dataset for benchmarking machine learning algorithms. *arXiv preprint arXiv:1708.07747* (2017).
- [65] XU, K., RUI, L., LI, Y., AND GU, L. Feature normalized knowledge distillation for image classification. In *Computer Vision–ECCV 2020: 16th European Conference, Glasgow, UK, August 23–28, 2020, Proceedings, Part XXV 16* (2020), Springer, pp. 664–680.
- [66] XU, Y., CUI, W., AND PEINADO, M. Controlled-channel attacks: Deterministic side channels for untrusted operating systems. In *IEEE Symposium on Security and Privacy* (2015).
- [67] YUE, X., DU, M., WANG, T., LI, Y., SUN, H., AND CHOW, S. S. Differential Privacy for Text Analytics via Natural Text Sanitization. *arXiv preprint arXiv:2106.01221* (2021).
- [68] ZAGORUYKO, S., AND KOMODAKIS, N. Paying more attention to attention: Improving the performance of convolutional neural networks via attention transfer. *arXiv preprint arXiv:1612.03928* (2016).
- [69] ZHANG, J., CHEN, C., AND LYU, L. IDEAL: Query-Efficient Data-Free Learning from Black-Box Models. In *The Eleventh International Conference on Learning Representations* (2022).
- [70] ZHANG, T., KISHORE, V., WU, F., WEINBERGER, K. Q., AND ARTZI, Y. BERTScore: Evaluating Text Generation with BERT, 2020.
- [71] ZHAO, W., PEYRARD, M., LIU, F., GAO, Y., MEYER, C. M., AND EGER, S. MoverScore: Text generation evaluating with contextualized embeddings and earth mover distance. In *Proceedings of the 2019 Conference on Empirical Methods in Natural Language Processing and the 9th International Joint Conference on Natural Language Processing (EMNLP-IJCNLP)* (Hong Kong, China, Nov. 2019), K. Inui, J. Jiang, V. Ng, and X. Wan, Eds., Association for Computational Linguistics, pp. 563–578.
- [72] ZHU, Y., YU, X., CHANDRAKER, M., AND WANG, Y.-X. Private-kNN: Practical Differential Privacy for Computer Vision. In *2020 IEEE/CVF Conference on Computer Vision and Pattern Recognition (CVPR)* (2020), pp. 11851–11859.

A Proof of ϵ -LDP with the Laplacian mechanism

We discuss the proof aforementioned in Section 3.2 here:

Theorem A.1. *LDPKiT's noise injection algorithm satisfies ϵ -LDP where $\epsilon = \frac{\Delta_f}{\lambda}$*

Proof. Let v be the original data and $f(v)$ be the query and computation function performed on the data with function sensitivity, $\Delta_f = \max_{v_1, v_2} \|f(v_2) - f(v_1)\|_1$. We define the randomization algorithm \mathcal{A} with Laplacian mechanism such that for any input value v , $\mathcal{A} = f(v) + \mathcal{Z}$, where \mathcal{Z} is sampled from the Laplacian distribution $L(z, \lambda)$ with scaling factor λ set to $\frac{\Delta_f}{\epsilon}$.

The probability that \mathcal{A} has an output $s \in \mathcal{S}$ given an input v can be expressed as:

$$\begin{aligned} \Pr[\mathcal{A}(v) = s] &= \Pr[f(v) + \mathcal{Z} = s] \\ &= \Pr[\mathcal{Z} = s - f(v)] \\ &= \frac{1}{2\lambda} \exp\left(-\frac{|s - f(v)|}{\lambda}\right) \end{aligned}$$

for all $s \in \mathcal{S}$.

To satisfy ϵ -LDP, we need Equation 1 to hold for any output $s \in \mathcal{S}$ and any input pairs v_1 and v_2 .

By substituting the PDF of Laplacian distribution's new expression into the Equation 1, we get

$$\frac{1}{2\lambda} \exp\left(-\frac{|s - f(v_1)|}{\lambda}\right) \leq e^\epsilon \frac{1}{2\lambda} \exp\left(-\frac{|s - f(v_2)|}{\lambda}\right)$$

which simplifies to

$$\exp\left(\frac{|s - f(v_2)| - |s - f(v_1)|}{\lambda}\right) \leq e^\epsilon$$

With $\lambda = \frac{\Delta_f}{\epsilon}$, the equation becomes:

$$\exp\left(\epsilon \cdot \frac{|s - f(v_1)| - |s - f(v_2)|}{\Delta_f}\right) \leq e^\epsilon \quad (4)$$

for all pairs of v_1 and v_2 .

Since $|s - f(v_1)| - |s - f(v_2)| \leq \Delta_f$ by the definition of sensitivity function, Equation 4 always holds.

□

B More discussion on ϵ -UMLDP

As described in Definition 3.3, we made some slight modifications to the ϵ -UMLDP formula from the original text sanitization paper [67]. In the original paper, the token sanitization probability controlled by the privacy budget, ϵ , is as follows:

$$\Pr[M(x) = y] = C \cdot \frac{\exp\left(-\frac{1}{2}\epsilon \cdot d_{\text{euc}}(\phi(x), \phi(y))\right)}{\sum_{y' \in V_N} \exp\left(-\frac{1}{2}\epsilon \cdot d_{\text{euc}}(\phi(x), \phi(y'))\right)} \quad (5)$$

In our paper, we remove the $\frac{1}{2}$ normalization factor before ϵ and more importantly, instead of *Euclidean Distance*, we use a scaled *Cosine Similarity* metric for token embedding distance measurement. Specifically,

$$d(\phi(x), \phi(y)) = 4 \left| \frac{1 - \exp(\text{Cosine_Sim}(\phi(x), \phi(y)) - 1)}{\exp(\text{Cosine_Sim}(\phi(x), \phi(y)) - 1)} \right| \quad (6)$$

We replace Euclidean Distance with Cosine Similarity because it is more commonly used in measuring the differences among embeddings in NLP tasks [26, 70, 71]. We scale the results of Cosine Similarity

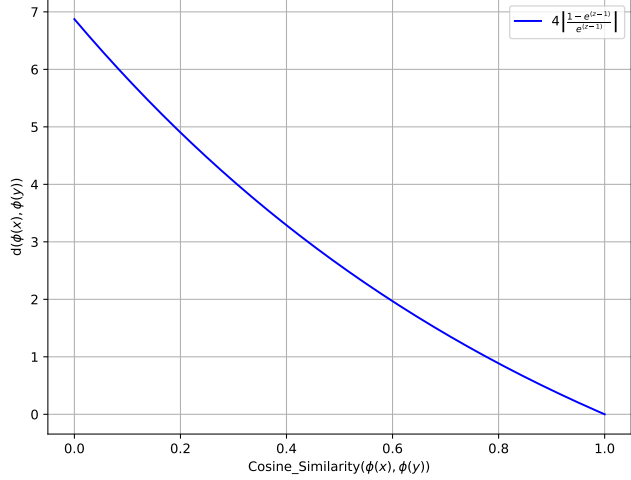


Figure 4: Relationship between the scaled cosine similarity and distance metrics of two token embeddings.

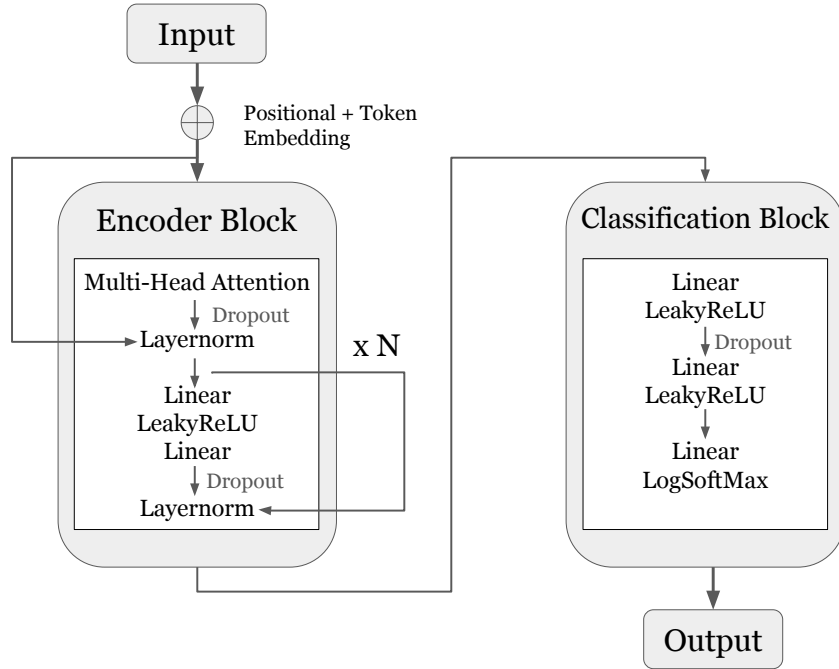


Figure 5: Encoder-based model architecture for the text modality.

between two embeddings with the function $4 \left| \frac{1 - \exp(Z-1)}{\exp(Z+1)} \right|$, where Z is $\text{Cosine_Sim}(\phi(x), \phi(y))$, so that the more similar two tokens, $\phi(x)$ and $\phi(y)$, are, the smaller $d(\phi(x), \phi(y))$ becomes, and the likelihood of replacement increases more drastically. Similarly, we penalize the dissimilar tokens to preserve utility. Figure 4 shows the scaled *Cosine Similarity* function. As the similarity approaches 1.0, $d(\phi(x), \phi(y))$ approaches zero. We do not need to worry about $d(\phi(x), \phi(y))$ becoming zero because the sets of sensitive and insensitive tokens are mutually exclusive. Same as the original paper, the likelihood of the replacement increases when the two tokens are more similar, i.e., $d(\phi(x), \phi(y))$ is smaller. We make the above changes so that the ϵ values we present in Section 4 are comparable to the values we use for image benchmarks. These changes do not augment the effect of the original ϵ -UMLDP implementation.

C Model architecture for text modality

Modern language models [62] can be categorized as encoder-based or decoder-based, depending on their specific applications. Encoder-based models (*e.g.*, BERT) are predominantly utilized for prediction/classification tasks by processing the embeddings. Conversely, decoder-based models (*e.g.*, GPT) can generate new sequences and are employed in applications like question answering and text summarization. Since this paper focuses on the classification task, we choose to use encoder-based Transformer architecture for the text modality evaluation. Figure 5 shows the detailed model architecture we use in our evaluation.

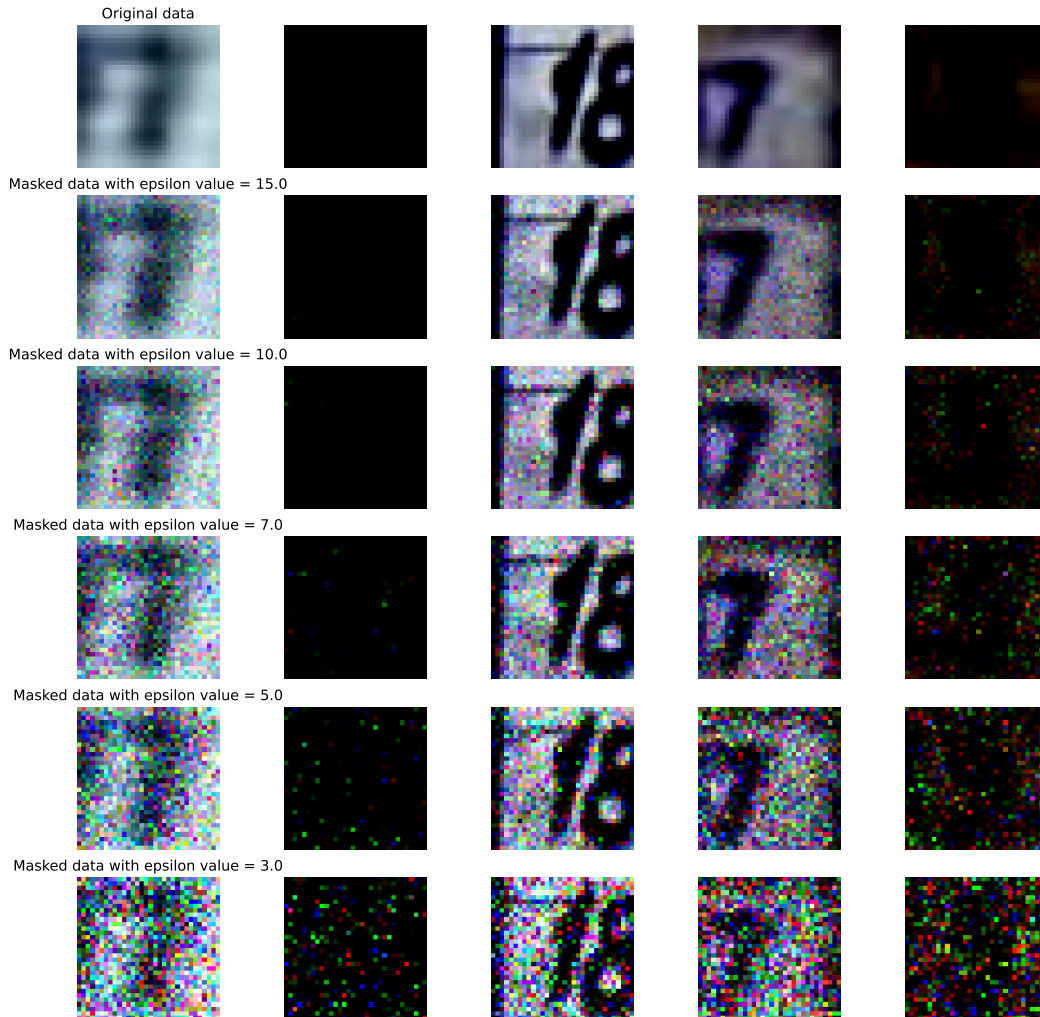


Figure 6: SVHN data samples with different noise levels.

Original: [‘[CLS]’, ‘i’, ‘feel’, ‘**sir**’, ‘**alex**’, ‘**ferguson**’, ‘is’, ‘a’, ‘keen’, ‘**admire**’, ‘##r’, ‘and’, ‘would’, ‘love’, ‘to’, ‘have’, ‘him’, ‘back’, ‘but’, ‘only’, ‘time’, ‘will’, ‘tell’, ‘[SEP]’]

Substituted ($\epsilon=15$): [‘[CLS]’, ‘i’, ‘feel’, ‘**##cia**’, ‘**##py**’, ‘**side**’, ‘is’, ‘a’, ‘keen’, ‘**close**’, ‘##r’, ‘and’, ‘would’, ‘love’, ‘to’, ‘have’, ‘him’, ‘back’, ‘but’, ‘only’, ‘time’, ‘will’, ‘tell’, ‘[SEP]’]

Figure 7: CARER text data sample with ϵ -UMLDP noise ($\epsilon = 15$).

Original: [‘[CLS]’, ‘i’, ‘feel’, ‘as’, ‘if’, ‘that’, ‘by’, ‘itself’, ‘would’, ‘ve’, ‘given’, ‘more’, ‘lyrical’, ‘##ly’, ‘talented’, ‘r’, ‘amp’, ‘b’, ‘artists’, ‘like’, ‘jill’, ‘scott’, ‘a’, ‘wider’, ‘platform’, ‘without’, ‘selling’, ‘out’, ‘on’, ‘what’, ‘they’, ‘believe’, ‘[SEP]’]

Substituted ($\epsilon=5$): [‘[CLS]’, ‘i’, ‘feel’, ‘as’, ‘if’, ‘that’, ‘by’, ‘itself’, ‘would’, ‘ve’, ‘given’, ‘more’, ‘won’, ‘##ly’, ‘talented’, ‘r’, ‘amp’, ‘b’, ‘artists’, ‘like’, ‘travel’, ‘rid’, ‘a’, ‘increasingly’, ‘ask’, ‘without’, ‘current’, ‘out’, ‘on’, ‘what’, ‘they’, ‘believe’, ‘[SEP]’]

Figure 8: CARER text data sample with ϵ -UMLDP noise ($\epsilon = 5$).

Original: [‘[CLS]’, ‘i’, ‘feel’, ‘cause’, ‘all’, ‘of’, ‘the’, ‘most’, ‘amazing’, ‘poets’, ‘that’, ‘iv’, ‘##e’, ‘ever’, ‘and’, ‘when’, ‘i’, ‘use’, ‘the’, ‘word’, ‘poet’, ‘i’, ‘mean’, ‘ben’, ‘webster’, ‘or’, ‘billie’, ‘holiday’, ‘or’, ‘maya’, ‘pe’, ‘##lis’, ‘##ets’, ‘##kaya’, ‘or’, ‘the’, ‘incredible’, ‘carmen’, ‘ama’, ‘##ya’, ‘[SEP]’]

Substituted ($\epsilon=3$): [‘[CLS]’, ‘i’, ‘feel’, ‘cause’, ‘all’, ‘of’, ‘the’, ‘most’, ‘amazing’, ‘same’, ‘that’, ‘iv’, ‘##e’, ‘ever’, ‘and’, ‘when’, ‘i’, ‘use’, ‘the’, ‘word’, ‘some’, ‘i’, ‘mean’, ‘saying’, ‘iv’, ‘or’, ‘does’, ‘lou’, ‘or’, ‘##ant’, ‘warm’, ‘having’, ‘more’, ‘very’, ‘or’, ‘the’, ‘who’, ‘doomed’, ‘valuable’, ‘decided’, ‘[SEP]’]

Figure 9: CARER text data sample with ϵ -UMLDP noise ($\epsilon = 3$).

D Hyperparameter choices and dataset preparation

In this section, we document hyperparameter choices and dataset splits for the experiments in Section 4. For image modality, we train \mathcal{M}_R with a learning rate of 0.1 for 200 epochs on each dataset. \mathcal{M}_R is trained on 35k data points for CIFAR-10 and Fashion-MNIST, 48,257 data points for SVHN and 210k data points for CARER. \mathcal{D}_{priv} and \mathcal{D}_{val} are split from the remaining data points unseen by \mathcal{M}_R , where \mathcal{D}_{priv} is used to train and evaluate \mathcal{M}_L , and \mathcal{D}_{val} is used for pure model generalizability evaluation. Specifically, CIFAR-10 has 15k data points in \mathcal{D}_{priv} , Fashion-MNIST and SVHN have 25k, and CARER has 70k. As for \mathcal{D}_{val} , its size is 10k for both CIFAR-10 and Fashion-MNIST, 26,032 for SVHN, and 10k for CARER. We train \mathcal{M}_L in an iterative learning process instead of one-shot learning to study the effect of $|\mathcal{D}_{priv}|$. In each iteration, \mathcal{M}_L randomly selects 1.5k, 2.5k, and 2.5k data samples from \mathcal{D}_{priv} for CIFAR-10, Fashion-MNIST, and SVHN, respectively. Thus, the total number of iterations is 10 for all benchmarks to finish querying the entire \mathcal{D}_{priv} . The epoch number in each iteration is set to 100 for CIFAR-10 and Fashion-MNIST and 50 for SVHN. \mathcal{M}_L ’s learning rate is 0.1 for all image benchmarks. For text modality, we train \mathcal{M}_R and \mathcal{M}_L with a learning rate of 0.0001 for 20 epochs on CARER. \mathcal{M}_L randomly picks 7k data points from \mathcal{D}_{priv} in each iteration and trains for 20 epochs per iteration, 10 iterations in total, to query the entire 70k dataset split of \mathcal{D}_{priv} . If \mathcal{M}_L ’s training dataset is the entire noised \mathcal{D}_{priv} , eventually, \mathcal{M}_L is trained on 15k data points for CIFAR-10, 25k data points for Fashion-MINST and SVHN, and 70k data points for CARER. The final accuracies in Figures 2 and 3, Appendix F, as well as all the Zest distances, are reported assuming \mathcal{M}_L is trained on the entire split of \mathcal{D}_{priv} .

E Examples of data with LDP noise

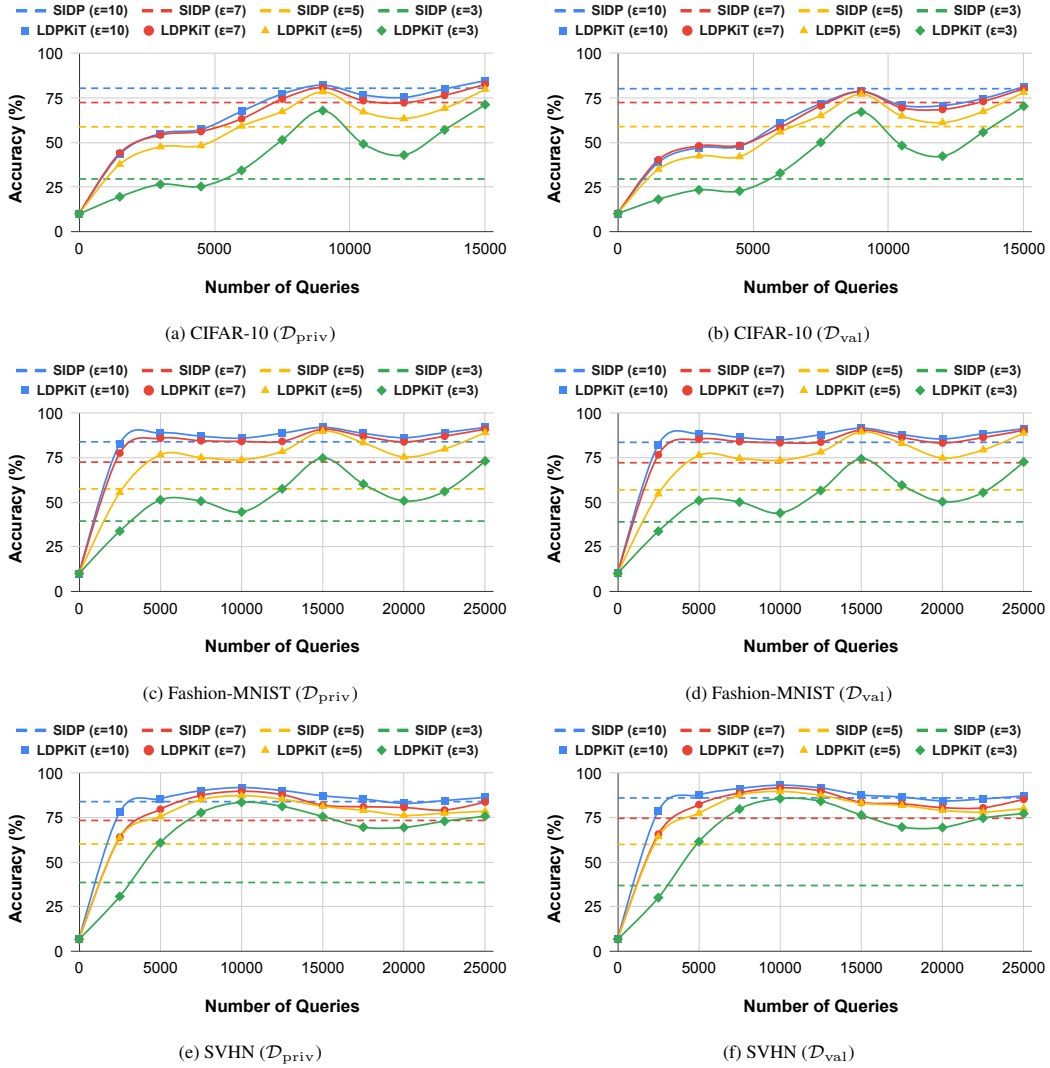
Figure 6 shows some SVHN image data samples with various ϵ -LDP noise applied. Figures 7, 8, and 9 show examples of CARER’s text inputs with substituted tokens for ϵ -UMLDP privacy guarantee.

F Additional experimental results

This section is complementary to the evaluation results presented in Section 4.

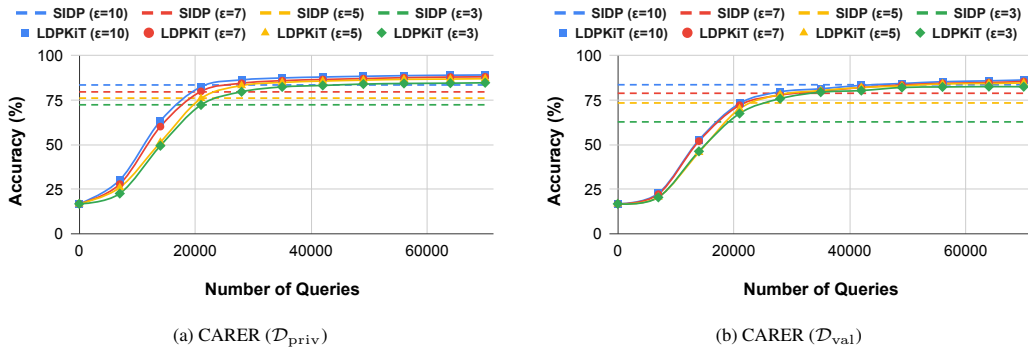
F.1 Additional accuracy plots on other models and datasets

We present MobileNetV2’s plots of accuracies on \mathcal{D}_{priv} and \mathcal{D}_{val} of various image benchmarks in Figure 10 and Transformer_EN1’s plots of accuracies on CARER in Figure 11.



SIDP lines in the plots give the average accuracy across all queries at a given ϵ .

Figure 10: MobileNetV2’s accuracies on $\mathcal{D}_{\text{priv}}$ and \mathcal{D}_{val} of CIFAR-10, Fashion-MNIST and SVHN.



SIDP lines in the plots give the average accuracy across all queries at a given ϵ .

Figure 11: Transformer_EN1’s accuracies on $\mathcal{D}_{\text{priv}}$ and \mathcal{D}_{val} of CARER emotion dataset.

Table 2: Comparison of final accuracies on $\mathcal{D}_{\text{priv}}$ between SIDP and LDPKiT.

Dataset	Model	Strategy	Accuracy on $\mathcal{D}_{\text{priv}}$ (%)				
			LDP ($\epsilon=15$)	LDP ($\epsilon=10$)	LDP ($\epsilon=7$)	LDP ($\epsilon=5$)	LDP ($\epsilon=3$)
CIFAR-10	ResNet-152	SIDP	84.78	80.46	72.42	58.76	29.46
	ResNet-18	LDPKiT	86.00 (± 0.13)	85.40 (± 0.06)	84.34 (± 0.15)	83.27 (± 0.25)	79.18 (± 0.11)
	MobileNetV2	LDPKiT	86.43 (± 0.03)	84.75 (± 0.18)	82.65 (± 0.24)	79.87 (± 0.82)	71.27 (± 0.53)
Fashion-MNIST	ResNet-152	SIDP	89.28	83.96	72.55	57.50	39.41
	ResNet-18	LDPKiT	93.10 (± 0.07)	92.77 (± 0.12)	92.43 (± 0.03)	91.73 (± 0.14)	80.03 (± 0.20)
	MobileNetV2	LDPKiT	92.53 (± 0.15)	92.05 (± 0.10)	91.10 (± 0.12)	89.17 (± 0.03)	73.17 (± 0.94)
SVHN	ResNet-152	SIDP	90.94	83.96	73.38	60.16	38.51
	ResNet-18	LDPKiT	92.17 (± 0.64)*	90.71 (± 0.85)	87.98 (± 0.78)	87.27 (± 1.07)	83.81 (± 1.16)
	MobileNetV2	LDPKiT	88.40 (± 0.63)	86.33 (± 2.15)*	83.74 (± 0.44)	78.54 (± 4.00)	75.77 (± 3.63)
CAREER	Transformer_EN2	SIDP	87.12	83.53	79.63	76.13	72.38
	Transformer_EN1	LDPKiT	89.86 ($\pm 1E-3$)	89.14 ($\pm 1E-3$)	88.11 ($\pm 2E-3$)	87.05 ($\pm 2E-3$)	84.75 ($\pm 4E-4$)

<Accuracy>* indicates that the accuracy has a $p > 0.05$. The values recorded in parentheses are the standard deviations of the accuracies.

Table 3: Comparison of final accuracies on \mathcal{D}_{val} between SIDP and LDPKiT.

Dataset	Model	Strategy	Accuracy on \mathcal{D}_{val} (%)				
			LDP ($\epsilon=15$)	LDP ($\epsilon=10$)	LDP ($\epsilon=7$)	LDP ($\epsilon=5$)	LDP ($\epsilon=3$)
CIFAR-10	ResNet-152	SIDP	84.13	80.20	72.43	58.89	29.44
	ResNet-18	LDPKiT	78.80 (± 3.15)*	81.60 (± 0.35)	81.80 (± 0.40)	81.60 (± 0.12)	78.27 (± 0.31)
	MobileNetV2	LDPKiT	81.81 (± 0.40)	81.31 (± 0.21)*	80.22 (± 0.38)	78.18 (± 1.19)	70.36 (± 0.44)
Fashion-MNIST	ResNet-152	SIDP	89.12	83.68	72.19	56.95	38.97
	ResNet-18	LDPKiT	92.94 (± 0.04)	92.46 (± 0.18)	92.18 (± 0.12)	91.43 (± 0.13)	79.85 (± 0.10)
	MobileNetV2	LDPKiT	91.86 (± 0.18)	91.34 (± 0.16)	90.50 (± 0.21)	88.83 (± 0.20)	72.65 (± 0.84)
SVHN	ResNet-152	SIDP	92.63	86.04	74.60	59.95	36.82
	ResNet-18	LDPKiT	93.12 (± 0.83)*	91.81 (± 0.34)	89.54 (± 0.87)	89.22 (± 1.59)	85.42 (± 1.46)
	MobileNetV2	LDPKiT	89.06 (± 0.47)	87.21 (± 2.33)*	85.29 (± 0.48)	80.13 (± 4.09)	77.26 (± 3.31)
CAREER	Transformer_EN2	SIDP	87.21	83.65	78.86	73.41	62.77
	Transformer_EN1	LDPKiT	87.09 ($\pm 2E-3$)*	86.34 ($\pm 1E-3$)	85.49 ($\pm 6E-3$)	84.64 ($\pm 5E-3$)	82.53 ($\pm 4E-3$)

<Accuracy>* indicates that the accuracy has a $p > 0.05$. The values recorded in parentheses are the standard deviations of the accuracies.

E.2 Final accuracy on $\mathcal{D}_{\text{priv}}$

Table 2 shows the tabulated final accuracies on $\mathcal{D}_{\text{priv}}$ of each dataset that LDPKiT and SIDP can achieve, which is also presented as bar graphs in Figure 2. We record the accuracies at the last epoch of training. The results draw the same conclusion as Section 4 that LDPKiT helps offset the accuracy trade-offs brought by LDP noise, and as more noise is added (*i.e.*, more privacy protection), the benefits become greater.

E.3 Final accuracy on \mathcal{D}_{val}

Table 3 shows the tabulated final accuracies on \mathcal{D}_{val} of each dataset that LDPKiT and SIDP can achieve. We record the accuracies at the last epoch of training. It is expected that the accuracies in Table 3 are slightly lower than the accuracies on $\mathcal{D}_{\text{priv}}$ presented in Table 2 since \mathcal{M}_L is trained on the noised samples in $\mathcal{D}_{\text{priv}}$, whereas \mathcal{D}_{val} remains unseen by the \mathcal{M}_L all the time.

G Model extraction attack detection with Zest

According to the *Zest* paper [22], we detect model extraction in the following steps:

1. Calculate the Zest distance between the two models to compare, *i.e.*, $D_z(\mathcal{M}_R, \mathcal{M}_L)$, where \mathcal{M}_L is trained on the entire data split of the noisy $\mathcal{D}_{\text{priv}}$, disjunctive to \mathcal{M}_R 's training dataset.
2. Calculate a reference distance by computing the average distance between five pairs of the victim and extracted models, denoted as \mathcal{M}_V and \mathcal{M}_E , where \mathcal{M}_E are generated by training

Table 4: Normalized Zest distance results with l_1 distance metric on \mathcal{M}_R and \mathcal{M}_L .

Dataset	\mathcal{M}_R	\mathcal{M}_L	LDP ($\epsilon=15$)	LDP ($\epsilon=10$)	LDP ($\epsilon=7$)	LDP ($\epsilon=5$)	LDP ($\epsilon=3$)
CIFAR-10	ResNet-152	ResNet-18	1.5127 (± 0.16)	1.3763 (± 0.01)	1.4641 (± 0.04)	1.5061 (± 0.08)	1.5547 (± 0.10)
		MobileNetV2	1.1071 (± 0.03)	1.1733 (± 0.01)	1.2509 ($\pm 2E-3$)	1.3247 (± 0.11)	1.2687 (± 0.05)
Fashion-MNIST	ResNet-152	ResNet-18	1.3780 (± 0.16)	1.8360 (± 0.11)	2.1093 (± 0.16)	2.0301 (± 0.04)	2.0047 (± 0.10)
		MobileNetV2	1.1033 (± 0.07)	1.3135 (± 0.16)	1.6869 (± 0.06)	1.8960 (± 0.04)	1.7669 (± 0.08)
SVHN	ResNet-152	ResNet-18	1.0320 (± 0.05)	1.0314 (± 0.01)	1.0535 (± 0.03)	1.0829 (± 0.01)	1.1469 (± 0.04)
		MobileNetV2	1.0807 (± 0.01)	1.0693 (± 0.01)	1.1058 (± 0.04)	1.0980 (± 0.04)	1.1501 (± 0.01)

The values recorded in parentheses are the standard deviations of the accuracies.

Table 5: Normalized Zest distance results with l_2 distance metric on \mathcal{M}_R and \mathcal{M}_L .

Dataset	\mathcal{M}_R	\mathcal{M}_L	LDP ($\epsilon=15$)	LDP ($\epsilon=10$)	LDP ($\epsilon=7$)	LDP ($\epsilon=5$)	LDP ($\epsilon=3$)
CIFAR-10	ResNet-152	ResNet-18	1.4343 (± 0.13)	1.3124 (± 0.01)	1.3641 (± 0.03)	1.4047 (± 0.06)	1.4452 (± 0.08)
		MobileNetV2	1.0767 (± 0.02)	1.1165 (± 0.01)	1.1602 ($\pm 3E-3$)	1.1904 (± 0.03)	1.2326 (± 0.03)
Fashion-MNIST	ResNet-152	ResNet-18	1.2685 (± 0.11)	1.9216 (± 0.26)	2.2307 (± 0.15)	2.1528 (± 0.05)	2.1489 (± 0.14)
		MobileNetV2	1.0426 (± 0.05)	1.2555 (± 0.11)	1.5792 (± 0.08)	1.7427 (± 0.02)	1.7056 (± 0.07)
SVHN	ResNet-152	ResNet-18	1.0570 (± 0.05)	1.0505 (± 0.01)	1.0520 (± 0.02)	1.0935 (± 0.01)	1.1600 (± 0.03)
		MobileNetV2	1.1115 ($\pm 1E-3$)	1.1062 (± 0.03)	1.1332 (± 0.05)	1.1405 (± 0.02)	1.1859 (± 0.01)

The values recorded in parentheses are the standard deviations of the accuracies.

Table 6: Normalized Zest distance results with l_∞ distance metric on \mathcal{M}_R and \mathcal{M}_L .

Dataset	\mathcal{M}_R	\mathcal{M}_L	LDP ($\epsilon=15$)	LDP ($\epsilon=10$)	LDP ($\epsilon=7$)	LDP ($\epsilon=5$)	LDP ($\epsilon=3$)
CIFAR-10	ResNet-152	ResNet-18	1.1639 (± 0.04)	1.0675 (± 0.05)	0.9643 (± 0.05)	0.9882 (± 0.07)	1.0402 (± 0.07)
		MobileNetV2	1.1075 (± 0.03)	1.1134 (± 0.08)	1.0206 (± 0.06)	1.2584 (± 0.27)	1.4150 (± 0.17)
Fashion-MNIST	ResNet-152	ResNet-18	1.2728 (± 0.17)	2.8362 (± 0.62)	3.4297 (± 0.38)	3.4847 (± 0.27)	2.9132 (± 0.22)
		MobileNetV2	1.1268 (± 0.01)	1.7314 (± 0.29)	1.8584 (± 0.40)	1.7269 (± 0.14)	2.0246 (± 0.10)
SVHN	ResNet-152	ResNet-18	1.1684 (± 0.07)	1.1758 (± 0.09)	1.0846 (± 0.11)	1.1766 (± 0.09)	1.2666 (± 0.13)
		MobileNetV2	1.3340 (± 0.28)	1.5230 (± 0.48)	1.2335 (± 0.20)	1.5855 (± 0.14)	1.6242 (± 0.19)

The values recorded in parentheses are the standard deviations of the accuracies.

Table 7: Final accuracy comparisons of training on noisy data versus original (noise-free) data of CIFAR-10 with ResNet-152 (\mathcal{M}_R) and ResNet-18 (\mathcal{M}_L).

Dataset Type	Strategy	Accuracy, Acc (%)				
		LDP ($\epsilon=15$)	LDP ($\epsilon=10$)	LDP ($\epsilon=7$)	LDP ($\epsilon=5$)	LDP ($\epsilon=3$)
\mathcal{D}_{priv}	SIDP	84.78	80.46	72.42	58.76	29.46
	LDPKiT with Training on Noised Data	86.00 (± 0.13)	85.40 (± 0.06)	84.34 (± 0.15)	83.27 (± 0.25)	79.18 (± 0.11)
	LDPKiT with Training on Original Data	85.92 (± 0.04)	83.14 (± 0.08)	77.66 (± 0.25)	67.28 (± 0.04)	38.74 (± 0.46)
\mathcal{D}_{val}	SIDP	84.13	80.20	72.43	58.89	29.44
	LDPKiT with Training on Noised Data	78.80 (± 3.15)	81.60 (± 0.35)	81.80 (± 0.40)	81.60 (± 0.12)	78.27 (± 0.31)
	LDPKiT with Training on Original Data	78.81 (± 0.48)	77.77 (± 0.81)	74.39 (± 0.76)	64.33 (± 0.49)	35.65 (± 0.71)

The values recorded in parentheses are the standard deviations of the accuracies.

on \mathcal{M}_V 's labeled training dataset, *i.e.*,

$$D_{ref} = \frac{1}{5} \sum_{i=1}^5 D_z(\mathcal{M}_{Vi}, \mathcal{M}_{Ei}).$$

Here, \mathcal{M}_V has the same model architecture as \mathcal{M}_R , and \mathcal{M}_E has the same model architecture as \mathcal{M}_L , but trained on the same dataset as \mathcal{M}_V , rather than the noisy \mathcal{D}_{priv} .

3. Calculate the normalized Zest distance, *i.e.*, $\overline{D}_z = \frac{D_z}{D_{ref}}$.
4. Determine the existence of model extraction by comparing \overline{D}_z with *threshold* 1.

$\overline{D_z} < 1$ indicates \mathcal{M}_R and \mathcal{M}_L are similar models and model extraction occurs.
 $\overline{D_z} > 1$ indicates \mathcal{M}_R and \mathcal{M}_L are dissimilar, and thus no model extraction attack exists.

H Zest distances supplementary results

Since the authors claim that the Cosine Distance is the most accurate metric [22], we show the Cosine Distance measurement in the main paper. Here, we provide additional experimental results of Zest distance with l_1 , l_2 and l_∞ distance metrics in Tables 4, 5 and 6. This is an extension of the experiments in Section 4.4 to quantitatively show that the type of knowledge distillation in LDPKiT does not construct an adversarial model extraction attack.

I Study on training \mathcal{M}_L with noisy versus original data samples

This section is an extension of the discussion in Section 5. In addition to Section 4’s experimental results on CIFAR-10, we also record the accuracies on $\mathcal{D}_{\text{priv}}$ and \mathcal{D}_{val} at the last epoch of training in LDPKiT when training is done on original data samples from CIFAR-10 with ResNet-152 (\mathcal{M}_R) and ResNet-18 (\mathcal{M}_L). We keep all the parameters and hyperparameters the same. The accuracies are still collected based on \mathcal{M}_L ’s prediction on the original (noise-free) data samples in $\mathcal{D}_{\text{priv}}$ and \mathcal{D}_{val} , same as the evaluations in Section 4. The only difference in setting is whether or not we train \mathcal{M}_L with noisy data. As Table 7 shows, LDPKiT has higher accuracies in all noise levels when training is done on noisy data and noisy labels returned from \mathcal{M}_R , except for the $\epsilon = 15$ case on \mathcal{D}_{val} where privacy protection is the weakest with the least noise added. Therefore, training with noise² is the design choice we follow in the main paper.